JAM CM Journal of Applied Mathematics and Computational Mechanics 2026, 25(2), 98-114
www.amcm.pcz.pl p-ISSN 2299-9965
DOI: 10.17512/jamcm.2026.2.07 e-ISSN 2353-0588

NUMERICAL MODELING OF VISCOUS MHD FLOW INDUCED BY STRETCHING AND ROTATION IN COAXIAL CYLINDERS

Soner Aydinlik

Department of Mathematics, Faculty of Science and Letters, Istanbul Technical University
Istanbul, Turkey
aydinliks@itu.edu.tr

Received: 15 March 2026; Accepted: 11 May 2026

Abstract. In this study, the effect of viscous forces on magnetohydrodynamic (MHD) flow between two coaxial cylinders is investigated, where the inner cylinder undergoes linear axial stretching while the outer cylinder rotates with a constant angular velocity. A first-order slip boundary condition is imposed at the surface of the inner cylinder to account for the possibility of partial slip at the boundary. In addition, viscous dissipation is incorporated into the model to evaluate its contribution to the thermal behavior of the fluid. The governing partial differential equations for mass, momentum, and energy conservation are converted into a dimensionless system of ordinary differential equations by suitable transformations. The resultant equations are solved numerically with an efficient technique, specifically the Legendre Smooth Composite Pseudospectral Method. The influences of key parameters such as the curvature parameter, cylinder gap, magnetic parameter, and slip parameter are presented graphically, demonstrating that increasing the distance between the cylinders leads to higher fluid velocity and temperature levels. Furthermore, the results indicate the existence of a critical gap parameter at which the heat transfer rate reaches its minimum value. This observation provides useful physical insight for the optimal design of rotating cylindrical systems in engineering applications such as cooling devices, rotating machinery, and thermal energy transport systems.

MSC 2010: *65L12, 65L20, 76W05, 80M22*
Keywords: *magnetohydrodynamic (MHD) flow, viscous dissipation, heat transfer, coaxial cylinders, shifted Legendre polynomials*

Nomenclature

B_0	Magnetic field strength
c_p	Specific heat capacity of the fluid
Ec	Eckert number
$f(\eta)$	Dimensionless stream function
$f'(\eta)$	Dimensionless velocity component
Ha	Hartmann number
k	Thermal conductivity parameter
m	Magnetic interaction parameter
Nu	Nusselt number
p	Dimensional pressure
$P(\eta)$	Dimensionless pressure distribution
Pr	Prandtl number
q_w	Wall heat flux
r	Radial coordinate
Re	Reynolds number
T	Fluid temperature
T_w	Temperature at the cylinder surface
T_∞	Ambient fluid temperature
u, v	Velocity components in axial and radial directions
η_0	Dimensionless gap parameter between the cylinders
μ	Dynamic viscosity
ν	Kinematic viscosity
ρ	Fluid density
σ	Electrical conductivity
$\theta(\eta)$	Dimensionless temperature function
ω	Angular velocity of the outer cylinder

1. Introduction

Magnetohydrodynamic (MHD) flows play a significant role in engineering and industrial applications such as magnetic material processing, rotating machinery, and energy systems [1,2]. Flows in cylindrical and annular geometries are frequently encountered in systems including rotating shafts and turbines. For example, the steady torsional flow behavior of pseudoplastic fluids between rotating coaxial cylinders was investigated by Shaikh et al. [3]. Dou et al. [4] investigated the distribution of energy loss in Taylor-Couette flows and emphasized the importance of viscous friction.

Flows in coaxial cylindrical configurations have recently attracted attention due to their capability to control heat transfer characteristics. Turkyilmazoglu and Pop [5] investigated the transport phenomena induced by the axial stretching of an inner cylinder placed inside a fixed outer coaxial cylinder in the absence of a magnetic field.

Bilal et al. [6, 7] examined the dynamics of magnetohydrodynamic (MHD) flow in stretching and rotating cylinders, taking viscous effects into account. In addition, the effects of Joule heating and variable viscosity on MHD Couette flow between concentric pipes were studied by Makinde and Eegunjobi, while Taiwo [9] analyzed vertical concentric annuli under the influence of a radial magnetic field. Non-Newtonian fluids inside rotating cylinders under the influence of a magnetic field were investigated by Dizaji et al. [10].

Viscous dissipation denotes the irreversible transformation of mechanical energy into thermal energy, particularly significant in flow regimes characterized by high velocity gradients [11]. In MHD convective flows, viscous dissipation together with the influence of Joule heating on the temperature distribution was examined [12]. In studies [13–15], slip boundary conditions were also incorporated into the model for micro-scale applications. In addition, the effects of slip parameters on momentum transport in the flow over cylinders under magnetic influence were investigated in [16, 17].

From a computational standpoint, the governing equations characterizing MHD flow and heat transfer in coaxial cylindrical configurations exhibit significant nonlinearity and strong coupling. Because of this, obtaining accurate numerical solutions remains challenging. Convergence problems or a lot of computer work may make traditional numerical methods less useful. Pseudospectral methods [18, 19], on the other hand, have attracted considerable attention because they are highly accurate and computationally efficient, especially for problems with smooth solutions. Furthermore, smooth composite pseudospectral formulations guarantee improved numerical stability and solution smoothness throughout computational subdomains, rendering them particularly suitable for intricate coupled boundary value problems [20–22].

Recent investigations have further advanced the understanding of magnetohydrodynamic flows in rotating and porous configurations. For instance, the behavior of non-Newtonian Bingham fluids subjected to magnetic fields and radial electric forces has been analyzed in rotating disk systems, demonstrating significant interactions between viscous effects and electromagnetic forces [23]. Moreover, the asymptotic characteristics of viscous MHD flow through porous-walled pipes have been examined to clarify the influence of magnetic fields on transport mechanisms in confined geometries [24]. These studies highlight the growing interest in complex MHD flow configurations and provide additional motivation for the present investigation of viscous magnetohydrodynamic flow induced by stretching and rotation in coaxial cylinders with slip and thermal effects.

This study focuses on the numerical analysis of viscous magnetohydrodynamic flow and heat transfer in coaxial cylinders and investigates the influence of physical parameters such as the inter-cylinder gap, magnetic field, slip coefficient, and viscous dissipation using an advanced pseudospectral method based on shifted Legendre polynomials. An error analysis and a convergence study are presented to evaluate the accuracy and effectiveness of the proposed numerical method.

The novelty of the present study lies in the combined investigation of viscous dissipation, slip boundary conditions, and rotational MHD effects in coaxial cylindrical configurations within a unified computational framework. From an engineering perspective, the identification of a critical gap parameter is important for the optimal design of rotating cylindrical systems, including cooling devices, heat exchangers, and thermal insulation applications. The present results provide physical insight into the selection of appropriate inter-cylinder spacing for controlling heat transfer performance. Furthermore, for the considered parameter ranges, the numerical simulations converge to a unique physically stable solution branch, while the investigation of possible multiple solutions under extended conditions remains a topic for future research.

2. Mathematical model

The problem considered in this study consists of a steady viscous fluid with electrical conductivity located between concentric cylinders, where the motion is generated by the stretching of the inner cylinder along its axis and the continuous rotation of the outer boundary at a constant angular velocity. This configuration is also investigated in [6] and is illustrated in Figure 1. A uniform magnetic field is applied in the radial direction, and the Lorentz force accounts for the influence of this magnetic field on the flow.

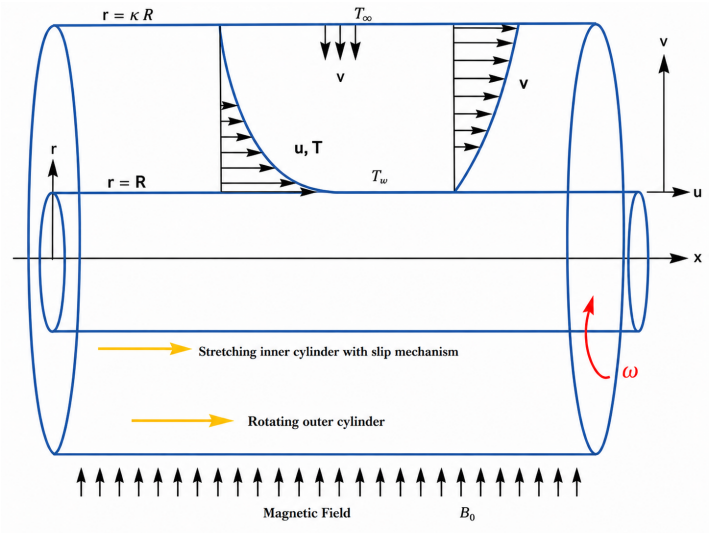

Fig. 1. Schematic diagram of the physical model showing the coaxial stretching and rotating cylinders under an applied magnetic field. Reproduced from [6]

The conservation of mass for the axisymmetric flow is expressed as

$$\frac{\partial}{\partial x}(ru)+\frac{\partial}{\partial r}(rv)=0, \tag{1}$$

where u and v denote the axial and radial velocity components, respectively.

The axial momentum balance, accounting for viscous diffusion and magnetic effects, is given by

$$u\frac{\partial u}{\partial x}+v\frac{\partial u}{\partial r}=\nu\left(\frac{1}{r}\frac{\partial}{\partial r}\left(r\frac{\partial u}{\partial r}\right)+\frac{\partial^2 u}{\partial x^2}\right)-\frac{\sigma\beta_0^2}{\rho}u, \tag{2}$$

while the radial momentum equation takes the form

$$u\frac{\partial v}{\partial x}+v\frac{\partial v}{\partial r}=-\frac{1}{\rho}\frac{\partial p}{\partial r}+\nu\left(\frac{1}{r}\frac{\partial}{\partial r}\left(r\frac{\partial v}{\partial r}\right)+\frac{\partial^2 v}{\partial x^2}-\frac{v}{r^2}\right). \tag{3}$$

The thermal behavior of the fluid, including the contribution of viscous dissipation, is described by the energy equation

$$u\frac{\partial T}{\partial x}+v\frac{\partial T}{\partial r}=\delta\left(\frac{1}{r}\frac{\partial}{\partial r}\left(r\frac{\partial T}{\partial r}\right)+\frac{\partial^2 T}{\partial x^2}\right)+\frac{\mu}{\rho c_p}\left(\frac{\partial u}{\partial r}\right)^2. \tag{4}$$

It should be noted that certain rotational effects such as centrifugal and Coriolis terms are not explicitly included in the present formulation. This simplification is based on the assumption of axisymmetric flow and moderate rotational intensity, for which the dominant influence of rotation is adequately represented through the imposed boundary motion of the outer cylinder. Such an approach is commonly adopted in the literature dealing with magnetohydrodynamic flow in cylindrical geometries, where the primary objective is to investigate the coupled effects of viscous dissipation, magnetic interaction, and slip boundary conditions under controlled rotational conditions.

The model incorporates a first-order slip mechanism on the surface of the internal cylinder, accompanied by a vanishing radial velocity condition. The temperature at the inner cylinder is assumed to be constant. These boundary conditions can be written as

$$\begin{aligned} u(r=R,x)&=ax+\alpha\nu\frac{\partial u}{\partial r},\\ v(r=R,x)&=0,\\ T(r=R,x)&=T_w. \end{aligned} \tag{5}$$

while at the outer rotating cylinder, the velocity and temperature conditions are given by

$$\begin{aligned} u(r=\kappa R,x)&=\Omega\kappa R,\\ T(r=\kappa R,x)&=T_\infty. \end{aligned} \tag{6}$$

Here, the velocity component v represents the radial velocity of the fluid, while the rotational motion of the outer cylinder is introduced through the tangential velocity imposed at the boundary. The present formulation assumes axisymmetric flow without an explicit azimuthal velocity component.

To transform the governing partial differential equations into a dimensionless form, the following similarity variables are introduced:

$$u = axf'(\eta), \qquad v = -\frac{\nu}{\gamma r} f(\eta),$$
$$p = \rho \left(\frac{\nu}{\gamma R}\right)^2 P(\eta), \tag{7}$$
$$\theta(\eta) = \frac{T - T_\infty}{T_w - T_\infty}, \qquad \eta = \frac{r^2 - R^2}{2\gamma R^2}.$$

Substituting these transformations into Eqs. (1)-(4) yields a set of coupled nonlinear ordinary differential equations governing the flow, pressure, and temperature fields:

$$f'^2 - ff'' = (2\gamma\eta + 1)f''' + 2\gamma f'' - mf', \tag{8}$$

$$P + f' + \frac{f^2}{2(2\gamma\eta + 1)} = P_0, \tag{9}$$

$$(2\gamma\eta + 1)\theta'' + 2\gamma\theta' = -Prf\theta' - Ec(2\gamma\eta + 1)(f'')^2. \tag{10}$$

The corresponding boundary constraints, expressed within the similarity domain, are defined as follows:

$$\begin{array}{ll} f'(0) = 1 + \lambda\gamma f''(0), & f'(\eta_0) = \omega, \\ f(0) = 0, & \theta(\eta_0) = 0. \\ \theta(0) = 1, & \end{array} \tag{11}$$

The physical characteristics of the flow are represented by the following dimensionless parameters identified in the governing equations:

$$Pr = \frac{\nu}{\delta}, \quad \delta = \frac{k}{\rho c_p}, \quad m = \frac{\sigma\beta_0^2}{\rho a}, \quad Ec = \frac{u_w^2\mu}{k(T_w - T_\infty)}, \tag{12}$$

with

$$\lambda = a\alpha r, \quad \omega = \frac{\Omega\kappa R}{ax}, \quad \gamma = \sqrt{\frac{\nu}{aR^2}}, \quad \eta_0 = \frac{\kappa^2 - 1}{2\gamma}. \tag{13}$$

3. Shifted Legendre smooth composite pseudo spectral method

In the context of solving initial or boundary value problems (IVP or BVP), one typically writes the approximation polynomial as,

$$y(x) = \sum_{n=0}^{N} a_n \varphi_n(x), \tag{14}$$

where

$$a_n = \frac{1}{\|\varphi_n\|^2} \sum_{j=0}^{N} \varphi_n(x_j)\, y(x_j)\, w_j. \tag{15}$$

In the above equation, N is polynomial degree, $\varphi_n(x)$ is an orthogonal polynomial, and w_j is the Gauss-Lobatto quadrature (GLQ) weight. In this study, shifted Legendre polynomials are used as trial functions in the pseudo spectral method. The shifted Legendre polynomials are introduced as

$$P_n^*(x) = \sum_{k=0}^{n} \frac{(-1)^{n+k}(n+k)!}{(n-k)!(k!)^2}(2x-1)^k, \tag{16}$$

respectively. The composite pseudo spectral methods are based on splitting the domain into the M-subdomains with the step size $h = \dfrac{(b-a)}{M}$. The collocation points are chosen as

$$x_k = \frac{x_k + 1}{2}, \quad \text{where} \quad (1 - {x_k}^2) P_N'(x_k) = 0, \quad k = 0, 1, \ldots, N. \tag{17}$$

The transformation to the j-th subdomain $\left[a + \dfrac{j(b-a)}{M},\ a + \dfrac{(j+1)(b-a)}{M}\right]$ is given as

$$t_{ki} = \frac{(b-a)}{M}\ (x_k + i), \quad i = 0, \ldots, M-1. \tag{18}$$

The numerical solutions for the i-th subdomain are defined as

$$y_i(x) = \sum_{n=0}^{N} a_{in} P_n^*(x) \tag{19}$$

where

$$a_{in} = \alpha_n \sum_{j=0}^{N} \frac{1}{(P_N^*(x_j))^2} y_i(x_j)\, P_n^*(x_j), \tag{20}$$

where

$$\alpha_n = \begin{cases} \dfrac{2n+1}{N(N+1)}, & n = 0,1,...,N-1, \\ \dfrac{1}{(N+1)}, & n = N. \end{cases} \tag{21}$$

The m-th order derivatives of the approximation polynomials at the nodes are

$$y_i^{(m)}(x_k) = \sum_{j=0}^{N} d_{k,j}^{(m)} y_i(x_j). \tag{22}$$

where

$$d_{k,j}^{(m)} = \frac{1}{(P_N^*(x_j))^2} \sum_{n=0}^{N} \alpha_n P_n^*(x_j) P_n^{*(m)}(x_k). \tag{23}$$

The expansion of (23) for Legendre is defined by [19]

$$d_{k,j}^{(m)} = \frac{1}{(P_N^*(x_j))^2} \sum_{n=0}^{N} \sum_{s=0}^{n} (-1)^{n+s} \frac{(x_i)^{s-m}(n+s)!}{\Gamma(s-m+1)(n-s)!(s!)} \alpha_n P_n^*(x_j) P_n^{*(m)}(x_k). \tag{24}$$

For smoothness,

$$y_{i+1}^{(r)}(x_0) = y_i^{(r)}(x_N). \quad r = 0,1,...,\lfloor m-1 \rfloor \tag{25}$$

must be satisfied. The present method reduces the problem to a set of algebraic equations. Combining the approximation polynomials for each subdomain, $y_i(x)$ yields the general solution, $P_N(x) \in C^{\lfloor m-1 \rfloor}[a,b]$.

4. Convergence and error analyses of Legendre SCPSM

4.1. Convergence analysis

Theorem 1 *Let $y_i(x)$ be a continuous function on $[0,1]$ and $\left|y_i^{(m)}(x)\right| \leq C_i$. Then, the equation* (14) *converges uniformly to the function $y_i(x)$, when $N \to \infty$ [19]. Thus, $y(x) = \bigcup_{i=1}^{M} y_i(x)$ also converges.* □

The proof of Theorem 1 is provided in Appendix A.

4.2. Error analysis

Theorem 2 *Assume that the approximation polynomial for i-th subinterval is defined by* $P_N y_i = \sum_{n=0}^{N} a_{in} P_n^*(x)$. *The error is presented as*

$$\|y_i - P_N y_i\| \leq \mathrm{O}(\frac{1}{N^{m-2}}) \tag{26}$$

for $\forall y_i(x) \in H_w^m[0,1]$, $m \geq 0$ *[19].* □

The detailed derivation of the error bound presented in Theorem 2 is given in Appendix A for completeness.

5. Numerical illustrations

In this section, the numerical results obtained from the proposed shifted Legendre smooth composite pseudospectral method are presented and discussed in detail. The accuracy and stability of the numerical scheme are first examined through the evaluation of the residual errors associated with the governing momentum and energy equations. Subsequently, the effects of the key physical parameters on the flow, thermal, and pressure fields are analyzed graphically. Unless otherwise stated, the results depicted in Figures 3-8 are computed for $\gamma = 0.5$, $\omega = 0.5$, $\lambda = 0.6$, $m = 0.3$, $Pr = 7$, $Ec = 0.1$, $P_0 = 0$, and $\eta_0 = 1$.

The accuracy of the numerical solution is assessed by evaluating the absolute residual errors $R_1(\eta)$ and $R_2(\eta)$, which are expected to approach zero throughout the computational domain.

$$\begin{aligned} R_1(\eta) &= \left|(2\gamma\eta+1)f''' + 2\gamma f'' - mf' - \left(f'^2 - ff''\right)\right|, \\ R_2(\eta) &= \left|(2\gamma\eta+1)\theta'' + 2\gamma\theta' + Prf\theta' + Ec(2\gamma\eta+1)(f'')^2\right|. \end{aligned} \tag{27}$$

Figure 2 illustrates the numerical stability and convergence behavior of the present composite pseudospectral scheme through the residual errors R_1 and R_2, corresponding to Eqs. (8) and (10), respectively, for different values of the polynomial degree N and the number of subdomains M. It is clearly observed that increasing either N or M leads to a significant reduction in both residuals throughout the computational domain.

Table 1 shows that the present calculations are in good agreement with the results reported in [5] for the parameter values $\gamma = 0.5$, $\omega = 0$, $\lambda = 0$, $m = 0$, $Pr = 7$, and $Ec = 0$. To further validate the proposed method, Table 2 presents a comparison of the skin friction coefficient $-f''(0)$ with the results reported in Ref. [7], where one parameter is varied at a time while the others are kept fixed under the same parameter settings.

Figure 3 illustrates the influence of the gap parameter, η_0, on the dimensionless velocity f, the axial velocity gradient f', the temperature θ, and the pressure distribu-

tion P. As η_0 increases, corresponding to a widening of the annular region, noticeable increases are observed in f, f', and θ, whereas a decrease is observed in the pressure function P. This behavior can be attributed to the reduced viscous resistance resulting from the weaker confinement of the flow region and to the larger fluid volume, which allows greater storage of thermal energy, and the reduction in geometric restriction leads to less steep pressure gradients.

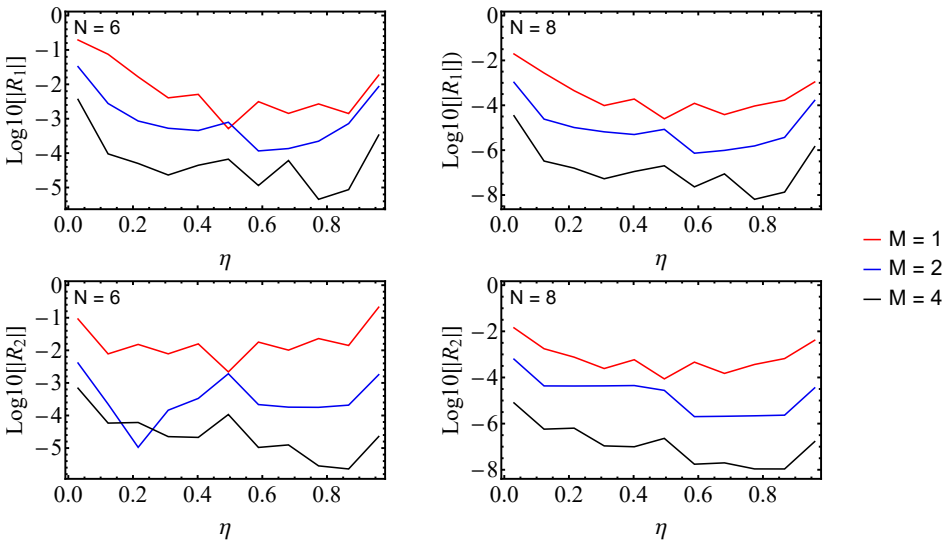

Fig. 2. Logarithmic plots of the residual functions R_1 and R_2 for different values of N and M

Table 1. Comparison of physical quantities for different values of η_0

	$\eta_0 = 0.5$		$\eta_0 = 1$		$\eta_0 = 1.92$		$\eta_0 = 5$	
	[5]	Present	[5]	Present	[5]	Present	[5]	Present
$-f''(0)$	2.62818	2.62818	1.72441	1.72441	1.36354	1.36352	1.20686	1.20507
$f(\eta_0)$	0.22834	0.22834	0.41437	0.41437	0.66852	0.66852	1.10140	1.10152
$-\theta'(0)$	2.85466	2.85466	2.14260	2.14260	2.01464	2.01464	2.04783	2.04749

Table 2. Comparison of the skin friction coefficient $-f''(0)$

Varied parameter	Value	[7]	Present method
γ	0.5	0.80101	0.80100
	1.0	0.57329	0.57322
ω	0.4	1.31470	1.31470
	0.8	0.61381	0.61381
λ	0.8	1.09162	1.09162
	1.0	1.04823	1.04824
M	0.8	1.21735	1.21735
	1.0	1.24823	1.24823

Figure 4 illustrates the influence of the curvature parameter γ on the flow and thermal characteristics. As γ increases, the viscous resistance becomes stronger, leading

to a reduction in fluid motion. Consequently, the velocity field weakens and both the velocity component $f(\eta)$ and the axial velocity gradient $f'(\eta)$ exhibit a decreasing trend. The reduction in flow velocity weakens convective heat transport, which results in lower temperature levels. In addition, the geometric constraints caused by curvature lead to higher pressure levels in the annular region.

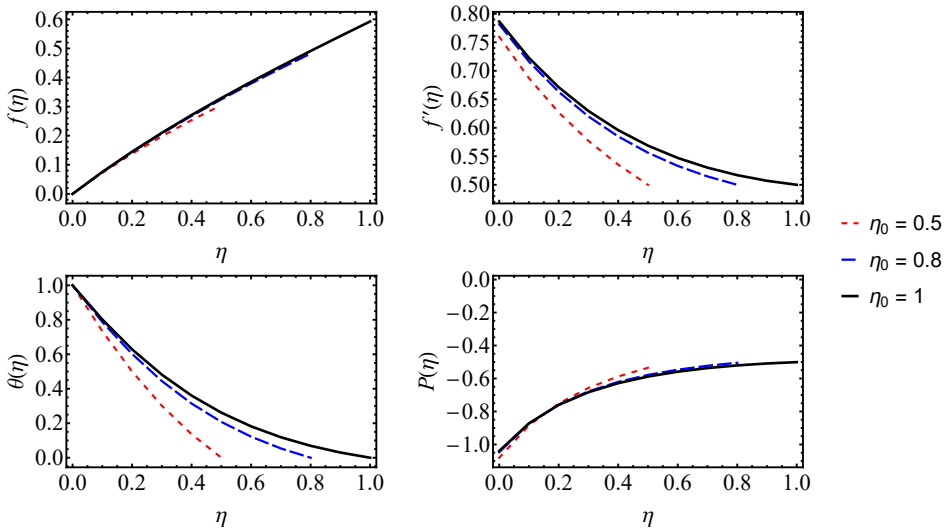

Fig. 3. Effect of the gap parameter η_0 on the velocity profiles $f(\eta)$ and $f'(\eta)$, dimensionless temperature $\theta(\eta)$ and pressure distribution $P(\eta)$

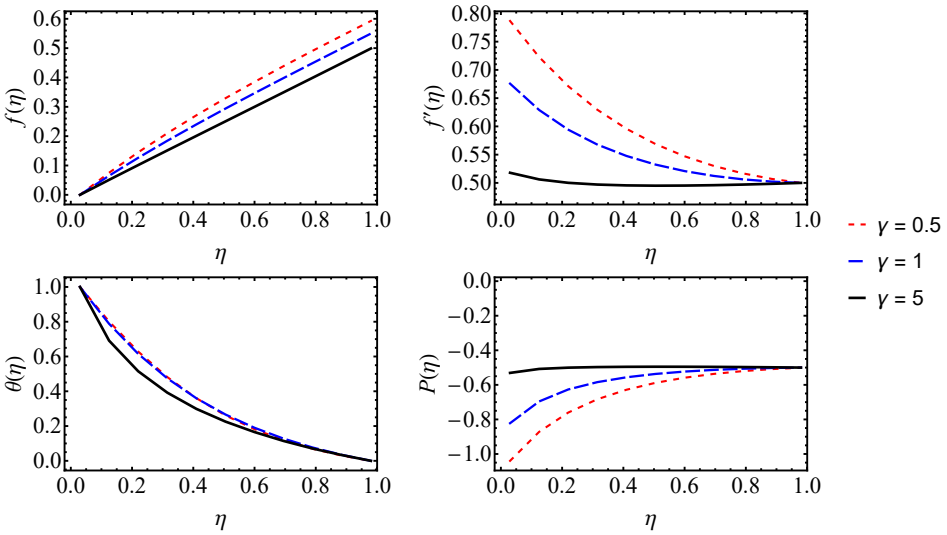

Fig. 4. Effects of the curvature parameter γ

Figure 5 shows how the slip parameter λ affects the fields of temperature, pressure, and velocity. As λ goes up, both f and f' go down. This means that a stronger slip makes it harder for the stretching inner cylinder to transfer momentum to the fluid. In contrast, as λ increases, both temperature θ and pressure P also increase. The lower flow intensity makes it harder for heat to escape, which raises the temperature. At the same time, the changed balance of forces in the flow causes the pressure in the flow domain to increase.

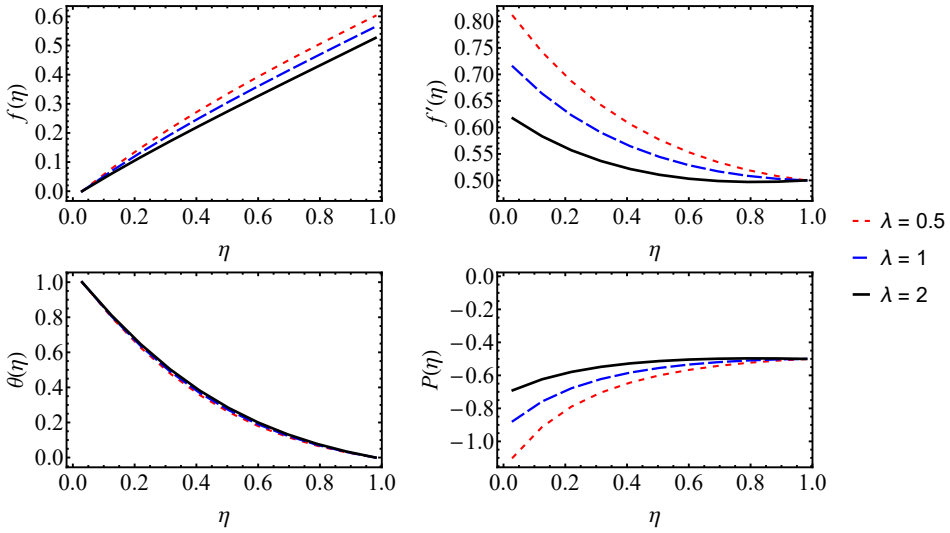

Fig. 5. Effects of the slip parameter λ

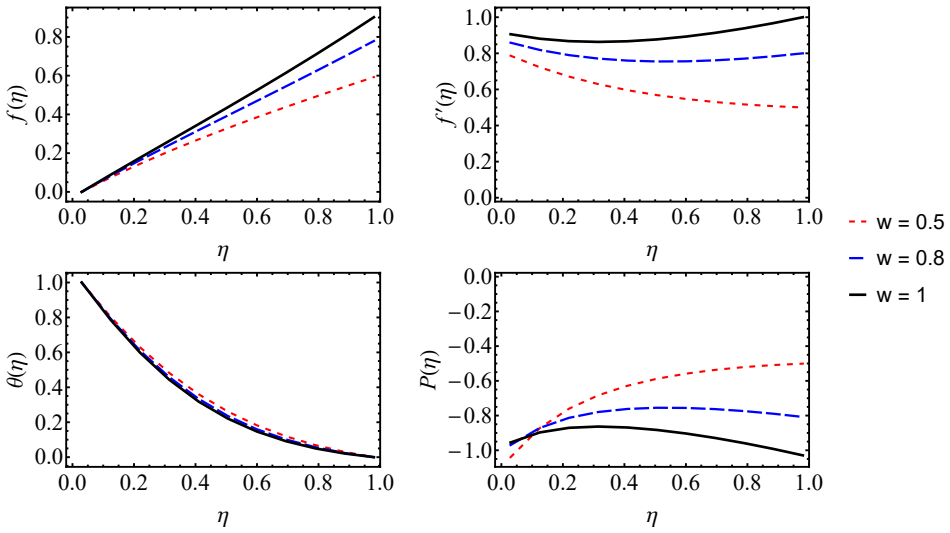

Fig. 6. Effects of the rotation parameter ω

The influence of the rotation parameter ω is illustrated in Figure 6. As the value of ω increases, the enhanced rotational effect of the outer cylinder accelerates the fluid motion, leading to an increase in both f and f', while the temperature θ and pressure P decrease.

Figure 7 illustrates the influence of the magnetic parameter m on the flow and heat transfer characteristics. As the value of m increases, the velocity functions f and f' decrease due to the strengthening of the Lorentz force induced by the magnetic field. In addition, a slight increase is observed in the temperature profile θ and the pressure P as a consequence of the magnetic damping effect.

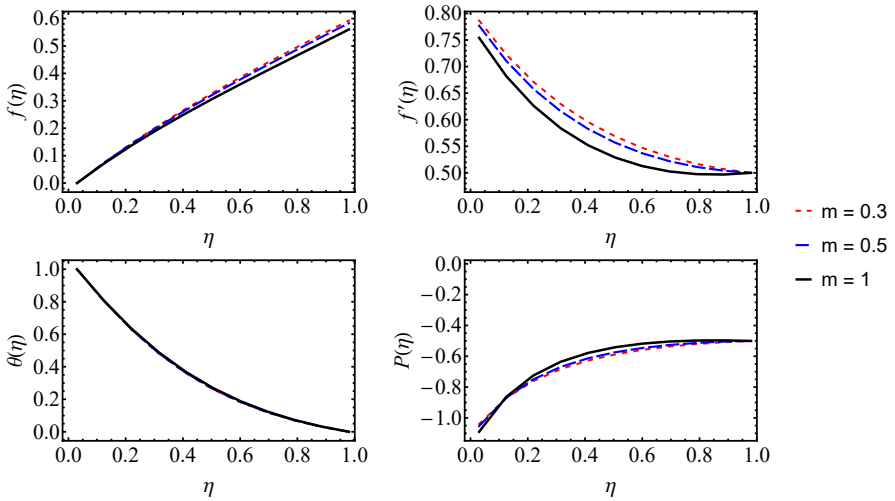

Fig. 7. Effects of the magnetic parameter m

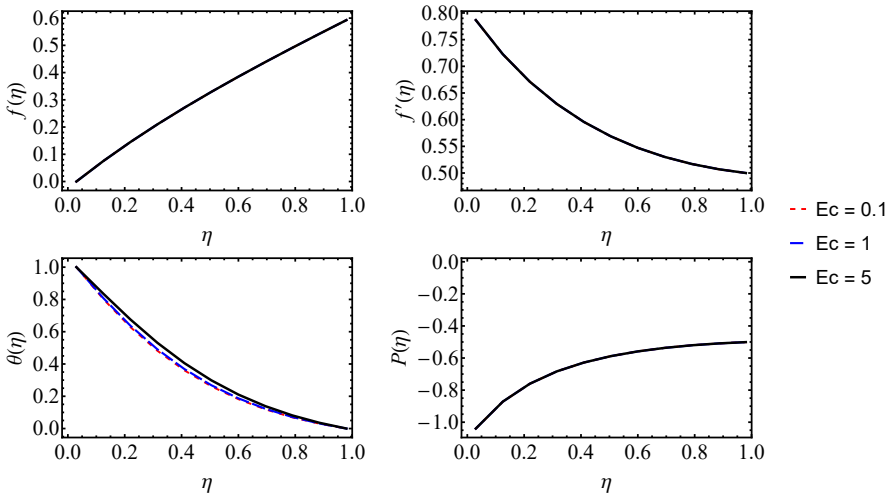

Fig. 8. Effects of the Eckert number Ec

Lastly, the influence of the Eckert number (Ec), which represents viscous dissipation, is presented in Figure 8. It is noted that augmenting Ec exerts an insignificant

effect on the velocity components f and f', as well as the pressure P. A small rise in the temperature θ, on the other hand, is noticed. This behavior is physically expected because viscous dissipation converts kinetic energy into thermal energy without significantly altering the momentum field. This causes a small rise in temperature while leaving the velocity structure almost unchanged.

6. Conclusions

In this study, the influence of viscous forces and slip conditions on magnetohydrodynamic (MHD) flow between coaxial cylinders is investigated. The flow is generated by the stretching of the inner cylinder along its axis and the rotation of the outer cylinder at a constant angular velocity, and the flow behavior is governed by the geometry of the cylinders, magnetic effects, and temperature. The cylinder gap, curvature parameter, magnetic parameter, slip parameter, angular velocity, Eckert number, and Prandtl number are considered as the governing parameters of the system.

The numerical results reveal the effects of the investigated parameters on the flow and heat transfer characteristics. An increase in the angular velocity of the outer cylinder enhances the fluid velocity, does not significantly alter the temperature distribution, but leads to an increase in the Nusselt number. As the magnetic parameter increases, the fluid motion slows down, resulting in a reduction in heat transfer efficiency. Increasing the slip parameter decreases the fluid velocity while increasing the Nusselt number and reducing the skin friction at the wall. An increase in the distance between the cylinders leads to higher velocity and temperature levels. In contrast, narrower gaps allow heat transfer to occur more effectively. As the cylinder curvature increases, both the fluid velocity and temperature decrease, and the critical gap value also shifts. An increase in the Eckert number raises the fluid temperature but does not significantly affect the wall shear stress. However, a slight decrease in the Nusselt number is observed.

The obtained results provide important insights into the interaction of viscous dissipation, slip conditions, and magnetohydrodynamic (MHD) forces in influencing the flow and heat transfer characteristics within coaxial cylinders. These findings are particularly significant for engineering applications where optimizing the spacing between cylinders, surface slip properties, and heat transfer performance is essential. The results also indicate the existence of a critical gap at which heat transfer reaches its minimum value, and further demonstrate that this critical gap shifts as the cylinder curvature increases.

From a practical engineering perspective, the identification of a critical gap parameter provides useful guidance for the optimal design of rotating cylindrical systems. In applications such as cooling devices, rotating machinery, heat exchangers, and thermal insulation systems, selecting an appropriate spacing between the cylinders can help control the heat transfer rate and improve the overall thermal performance of the system. Therefore, the present results offer a physically meaningful criterion for determining the optimal geometric configuration of coaxial cylindrical devices.

The present study focuses on the physically stable solution branch of the governing boundary value problem. For the considered range of physical parameters, the numerical simulations consistently converged to a unique solution, and no evidence of multiple solution branches was observed. The investigation of possible multiplicity of solutions under extended parameter regimes may be considered as an interesting direction for future research.

Declarations

Funding: This research was carried out with the assistance of Istanbul Technical University, under the funding framework of project TAB-2023-44975.

References

[1] Bég, O. Anwar (2003). *Giants of Engineering Science*. Matador, UK.

[2] Bég, O. Anwar, Ghosh, S.K., & Bég, T.A. (2011). *Applied Magnetofluid Dynamics: Modelling and Computation*. Lambert Academic Publishing, Germany.

[3] Shaikh, F., Shah, S.F., Siddiqui, A.M., & Kumar, L. (2022). Application of recursive approach of pseudoplastic fluid flow between rotating coaxial cylinders. *Alexandria Engineering Journal*, *61*(10), 7823-7832.

[4] Dou, H.S., Khoo, B.C., & Yeo, K.S. (2007). Energy loss distribution in the Plane Couette flow and the Taylor-Couette flow between concentric rotating cylinders. *International Journal of Thermal Sciences*, *46*(3), 262-275.

[5] Turkyilmazoglu, M., & Pop, I. (2023). Induced flow and heat transfer due to inner stretching and outer stationary coaxial cylinders. *International Communications in Heat and Mass Transfer*, *146*, 106903.

[6] Bilal, M., Nasr, E.A., ur Rahman, M., & Waqas, M. (2024). Numerical investigation of MHD hybrid nanofluid flow with heat transfer subject to thermal radiation across two coaxial cylinders. *Numerical Heat Transfer Part A. Applications*, *86*(1).

[7] Bilal, M., Khadim, S., & Mehmood, Y. (2025). Numerical analysis of MHD flow in coaxial stretching and rotating cylinders with viscous effect. *Zeitschrift für Angewandte Mathematik und Mechanik*, *105*, e202400945.

[8] Makinde, O.D., & Eegunjobi, A.S. (2020). Entropy analysis of a variable viscosity MHD Couette flow between two concentric pipes with convective cooling. *Engineering Transactions*, *68*(4), 317-334.

[9] Taiwo, Y.S. (2017). Exact solution of an MHD natural convection flow in vertical concentric annulus with heat absorption. *International Journal of Systems and Systems Engineering*, *1*(1), 15-24.

[10] Dizaji, A.F., Salimpour, M.R., & Jam, F. (2008). Flow field of a third-grade non-Newtonian fluid in the annulus of rotating concentric cylinders in the presence of magnetic field. *Journal of Mathematical Analysis and Applications*, *337*(1), 632-645.

[11] Mahmud, S., & Fraser, R.A. (2002). Viscous dissipation effects in forced convection heat transfer. *International Journal of Thermal Sciences*, 41, 1-7.

[12] Raju, K.V.S., Reddy, T.S., Raju, M.C., Narayan, P.V.S., & Venkataraman, S. (2014). MHD convective flow through porous medium in a horizontal channel. *Ain Shams Engineering Journal*, *5*(2), 543-551.

[13] Karniadakis, G.E., Beskok, A., & Aluru, N. (2005). *Microflows and Nanoflows: Fundamentals and Simulation*. Springer, New York.

[14] Lauga, E., Brenner, M.P., & Stone, H.A. (2007). Microfluidics: The no-slip boundary condition. In: *Springer Handbook of Experimental Fluid Mechanics*, pp. 1219-1240. Springer.

[15] Gad-el-Hak, M. (2005). *MEMS: Introduction and Fundamentals*. CRC Press, Boca Raton.

[16] Mukhopadhyay, S. (2013). MHD boundary layer slip flow along a stretching cylinder. *Ain Shams Engineering Journal*, *4*(2), 317-324.

[17] Qasim, M., Khan, Z.H., Khan, W.A., & Shah, I.A. (2014). MHD boundary layer slip flow and heat transfer of ferrofluid along a stretching cylinder. *PLOS ONE*, *9*(1), e83930.

[18] Aydinlik, S. (2024). A novel approach for fractional model of water pollution management. *Journal of Industrial and Management Optimization*, *20*(12), 3617-3627.

[19] Abdelhakem, M., Abdelhamied, D., Alshehri, M.G., & El-Kady, M. (2021). Shifted Legendre fractional pseudospectral differentiation matrices. *Fractals*, *29*, 2240038.

[20] Aydinlik, S. (2022). An efficient method for oxygen diffusion in a spherical cell with nonlinear oxygen uptake kinetics. *International Journal of Biomathematics*, *15*, 2250019.

[21] Aydinlik, S., & Kiris, A. (2022). First order smooth composite Chebyshev finite difference method for solving coupled Lane-Emden problem. *MATCH Communications in Mathematical and in Computer Chemistry*, *87*, 463-476.

[22] Aydinlik, S., Kiris, A., & Roul, P. (2025). A novel computational strategy for solving electrohydrodynamic flow problem. *Soft Computing*, *29*, 5009-5023.

[23] Uygun, N., & Turkyilmazoglu, M. (2025). MHD non-Newtonian Bingham fluid flow and heat transfer over a rotating disk regulated by a uniform radial electric field. *International Journal of Heat and Fluid Flow*, *116*, 109899. DOI: 10.1016/j.ijheatfluidflow.2025.109899.

[24] Turkyilmazoglu, M., & Alotaibi, A. (2025). On the viscous flow through a porous-walled pipe: asymptotic MHD effects. *Microfluidics and Nanofluidics*, *29*, 33. DOI: 10.1007/s10404-025-02808-5.

Appendix A: Proofs of Convergence and Error Estimates

PROOF 4.1 By using the orthogonality property of the shifted Legendre polynomials, a_{in} can be expressed as

$$a_{in} = (2n+1)\int_0^1 y_i(x)P_n^*(x)dx. \tag{28}$$

By using integration by parts and recursion relation of Legendre polynomials

$$a_{in} = \frac{1}{2}\int_0^1 y_i{}'(x)\sigma_1(x)\,dx, \quad n \geq 1, \tag{29}$$

where $\sigma_1(x) = P_{n-1}^*(x) - P_{n+1}^*(x) \lesssim \mathrm{O}(n^0)$ and the same procedure is applied once more:

$$a_{in} = \frac{1}{2}\int_0^1 y_i{}''(x)\sigma_2(x)\,dx, \tag{30}$$

where $\sigma_2(x) = \dfrac{P_{n+2}^*(x) - P_n^*(x)}{4n+6} - \dfrac{P_n^*(x) - P_{n-2}^*(x)}{4n-2} \lesssim \mathrm{O}(n^{-1})$.
Performing the above procedures $(m-2)$ times gives

$$|a_{in}| \lesssim \mathrm{O}\left(\frac{1}{n^{m-1}}\right). \tag{31}$$

A similar procedure to the one in the Chebyshev method gives an upper bound for the approximation

$$|y_i(x)| = \left|\sum_{n=0}^{\infty} a_{in}P_n^*(x)\right| \leq \sum_{n=0}^{\infty}|a_{in}| \leq |a_{i0}| + \sum_{n=1}^{\infty}|a_{in}| < \infty, \tag{32}$$

Consequently, the solution is bounded by

$$|y(x)| \leq \max_{1\leq i\leq M}|y_i(x)| \leq \max_{1\leq i\leq M}\left(|a_{i0}| + \sum_{n=1}^{\infty}|a_{in}|\right) < \infty. \tag{33}$$

PROOF 4.2 Since

$$\|y_i - P_N\,y_i\| \leq \left|\sum_{n=N+1}^{\infty} a_n P_n^*(x)\right| \leq \left|\sum_{n=N+1}^{\infty} a_n\right|, \tag{34}$$

then considering (34) with the integral test for series, we obtain

$$\|y_i - P_N\,y_i\| = \int_{N+1}^{\infty} a(x)dx \leq \mathrm{O}\left(\frac{1}{N^{m-2}}\right). \tag{35}$$